Supporting Information

Method for fabricating highly crystalline polyvinylidene fluoride for piezoelectric energy-harvesting and vibration sensor applications

Nirmal Prashanth Maria Joseph Raj, Abisegapriyan KS, Gaurav Khandelwal, Sang-Jae Kim*

Mailing address:

Nirmal Prashanth Maria Joseph Raj, Abisegapriyan KS, Gaurav Khandelwal, Sang-Jae Kim*

Nanomaterials & System Lab,

Major of Mechatronics Engineering,

Faculty of Applied energy system,

Jeju National University,

Jeju 63243, South Korea.

Email ID: nirmalpm@jejunu.ac.kr, abipriyan3@jejunu.ac.kr, gaurav@jejunu.ac.kr, kimsangj@jejunu.ac.kr

*Corresponding author

Experimental

Synthesis of $Bi_{0.5}Na_{0.5}TiO_3$ nanocubes (BNT NCs)

The hydrothermal synthesis was employed to prepare BNT cubes, and its schematically represented in Fig.S1. Initially, the 1:2 molar ratio of Bi source ($Bi(NO_3)_3.5H_2O$) to Ti source was ($Ti(OC_4H_9)_4$) was added to the distilled water and stirred for 10 minutes. Then, the two solutions were mixed together with the addition of 16 M NaOH, which acts as a Na source and controlling agent in the shape and size of the nanomaterials. After 1 hr stirring, the precursor solutions were loaded into the autoclave, and the reaction was performed at 200^oC for 80 hrs. Finally, the collected particles were washed multiple times and dried at 100^oC for about 5 hrs and later used in characterizations and film fabrications.

Measurement systems

The functional properties of the prepared PVFB films were analyzed by FTIR analysis by Compact FT-IR Spectrometer ALPHA II by Bruker in ATR mode between the range of 700 -1800 cm^{-1}. The structural properties of the synthesized $Bi_{0.5}Na_{0.5}TiO_3$ cubes were studied using an X-ray diffractometer (Empyrean by Malvern Panalytical) and Raman spectroscopy (LabRAM) with a laser wavelength of 514 nm and power of 10 mW with an ND filter of 10 %. The Piezo Force Microscopy (PFM) analyses were performed from a Scanning Probe Microscope (SPM) by Multimode 8 (Bruker). The prepared film's morphological analysis was analyzed using field-emission scanning electron microscopy (MIRA3 by TESCAN). The Keithley electrometer (6514) and current preamplifier (Stanford systems) were used to measure the electrical output responses of PVFB PENGs upon mechanical force. The constant mechanical force is generated by the linear motor (Lin Mot,

HF01-37 model). The bath sonicator cleaning unit Elmasonic P 30 H is used in the energy conversion and demonstrating the sensor applications.

Supporting Information

Figure S1 The schematic representation of $Bi_{0.5}Na_{0.5}TiO_3$ preparation through the hydrothermal reaction. **Figure S2** The structural analysis of the prepared $Bi_{0.5}Na_{0.5}TiO_3$ through XRD and Raman analysis. **Figure S3** The functional analysis by FTIR and the morphological analysis of the prepared PVFB film at ~ 30 % RH. **Figure S4** The morphological images of the prepared PVFB films with various loading of BNT at ~ 60 % RH. **Figure S5** The PFM phase and amplitude images of the 0 & 30 % PVFB film at 0 V bias. **Figure S6, S7** The repeatability and location varied PFM phase and amplitude loops of the 30 % PVFB film. **Figure S8** The electrical voltage and current outputs of various PVFB PENGs and switching polarity test output. **Figure S9** The cross-sectional SEM image of the 30 % PVFB film attached with the Al foil as electrodes with PDMS as supporting layer. **Figure S10** The 30 % PVFB PENG electrical current output under varying accelerations, commercial capacitor charging and discharging analysis. **Figure S11** The 30 % PVFB PENG electrical outputs under varying sonication power @ 37 kHz and three active modes of the bath sonicator. **Figure S12** The 30 % PVFB PENG electrical outputs under 100 W power @ 80 kHz and the schematic of device attachment positions to identify the high active region. **Figure S13** The electrical output of 30 % PVFB PENG under finger, hand and foot-tapping biomechanoid force conditions.

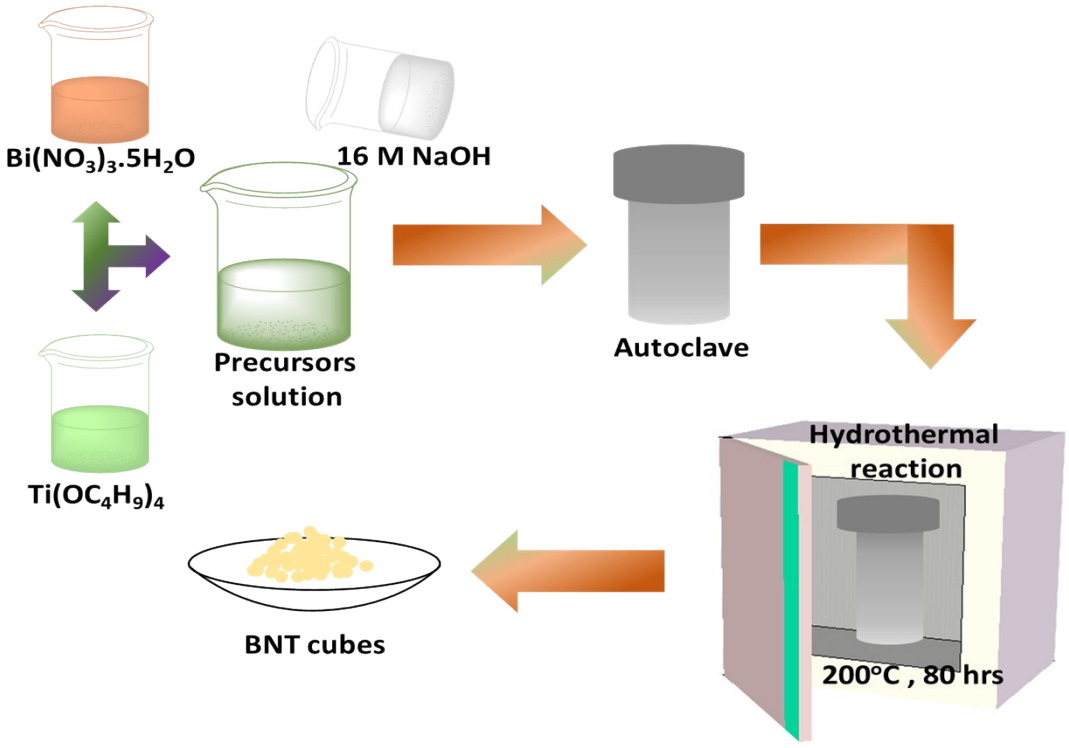

Figure S1 The schematic representation of $Bi_{0.5}Na_{0.5}TiO_3$ cubes preparation through the hydrothermal reaction.

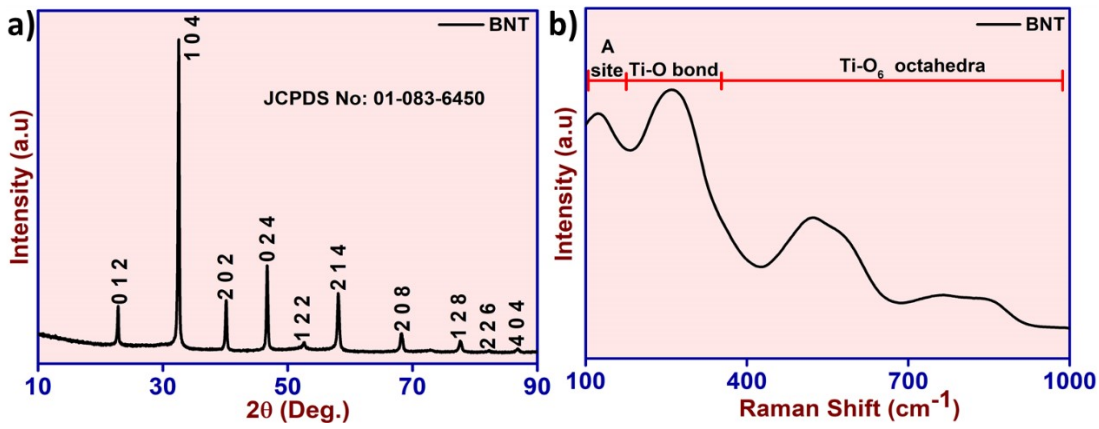

Figure S2 (a) The XRD pattern of the $Bi_{0.5}Na_{0.5}TiO_3$ cubes. (b) The Raman spectrum of the $Bi_{0.5}Na_{0.5}TiO_3$ cubes.

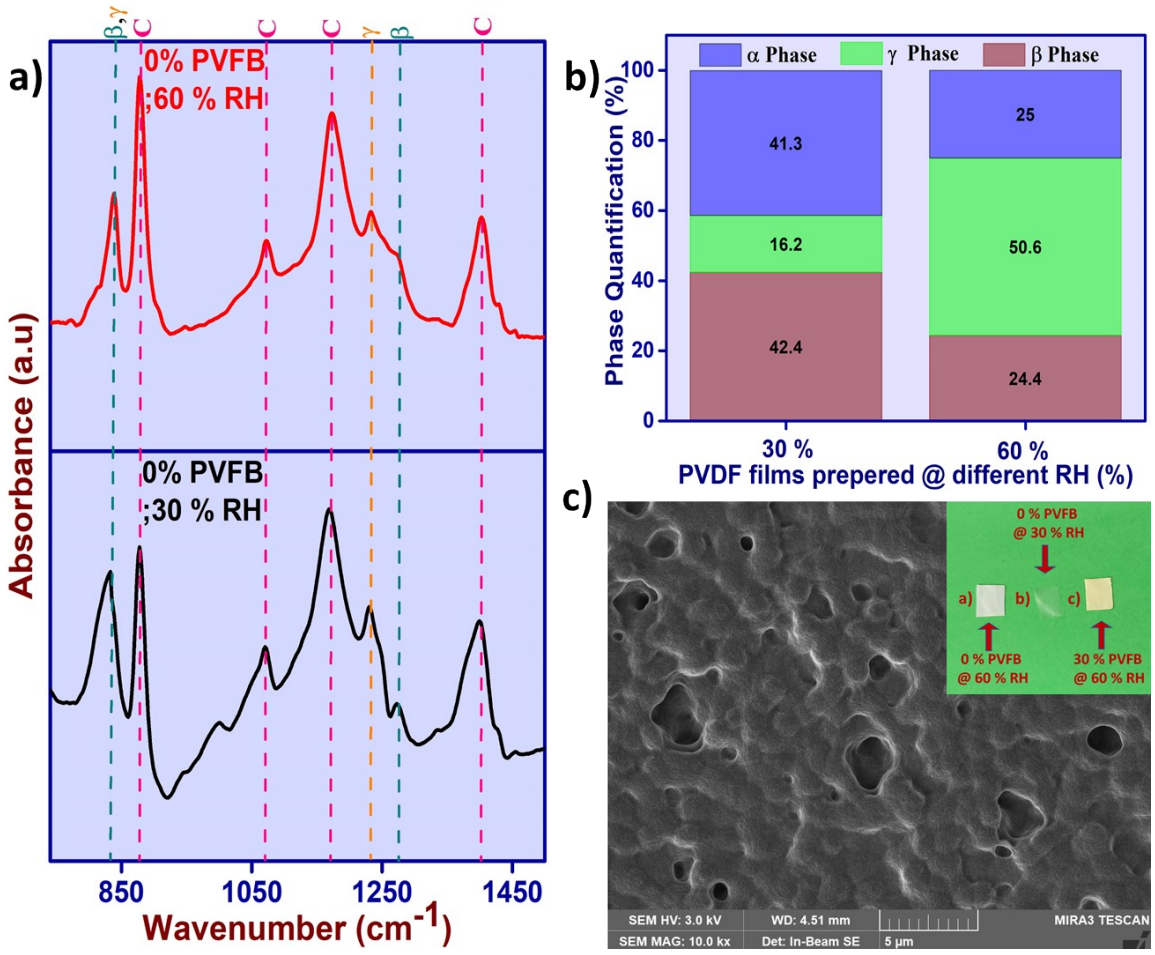

Figure S3 (a) The FTIR spectrum of 0 % PVFB film at 30 and 60 % relative humidity (RH). **(b)** The crystalline phase quantification of 0 % PVFB film at 30 and 60 % relative humidity (RH). **(c)** The morphological images of the 0 % PVFB films were prepared at 30 % relative humidity (RH). (Inset image: The digital images of PVFB films at different conditions)

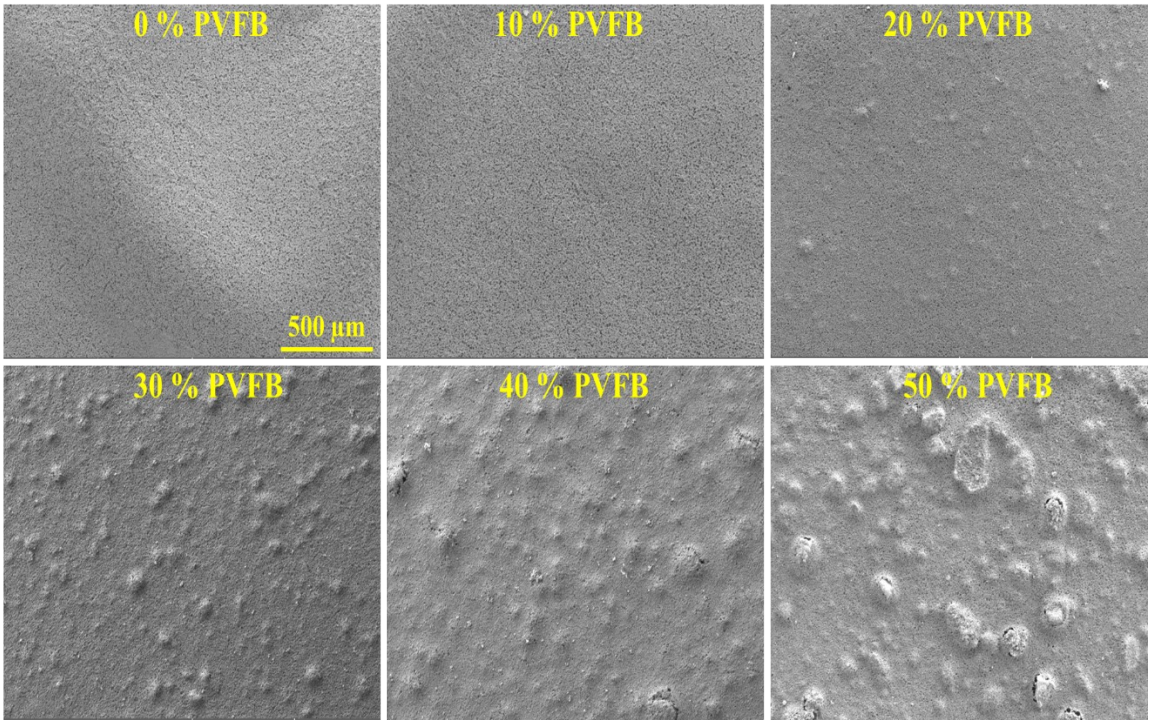

Figure S4 The morphological images of the various % of BNT cubes loaded PVFB films.

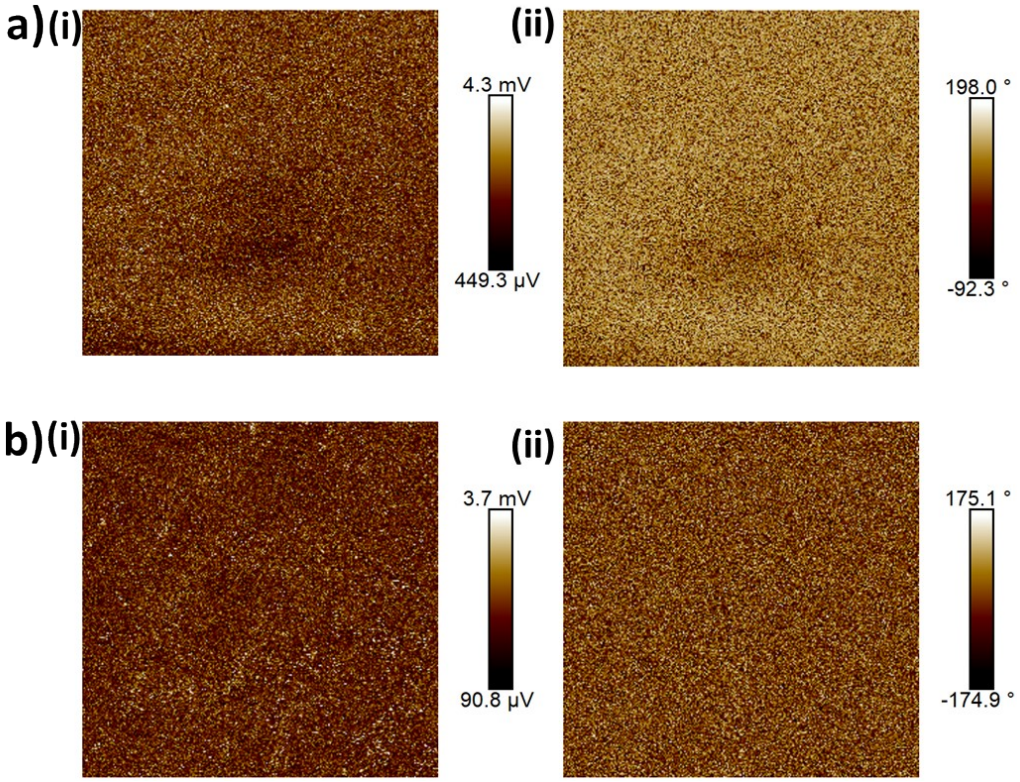

Figure S5 (a) The PFM amplitudes and phase images of the 0 % PVFB under 0 V bias. **(b)** The PFM amplitudes and phase images of the 30 % PVFB under 0 V bias.

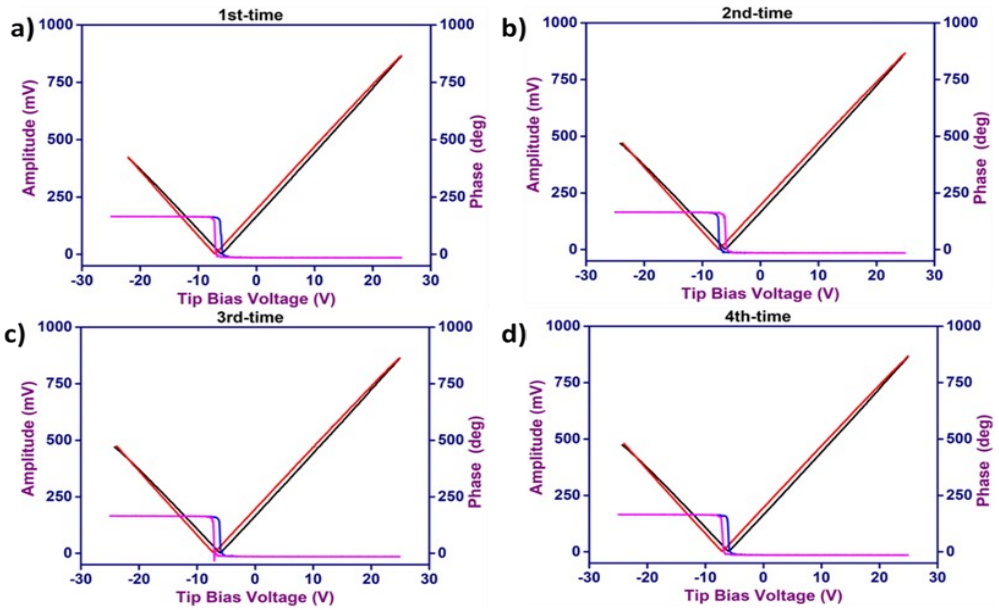

Figure S6 The repeatability test of 30 % PVFB films amplitude and phase loop.

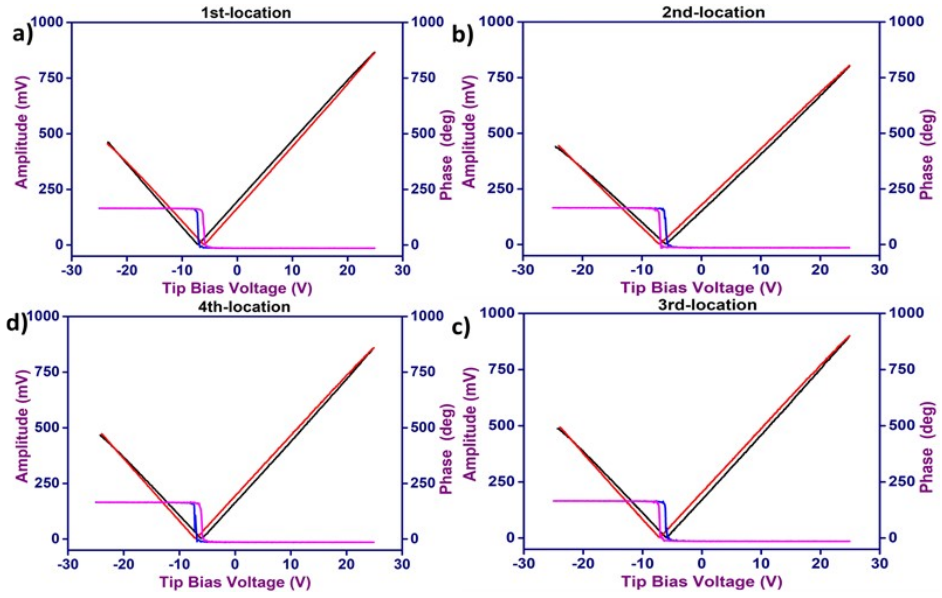

Figure S7 The reproducibility of 30 % PVFB films amplitude and phase loop at different locations.

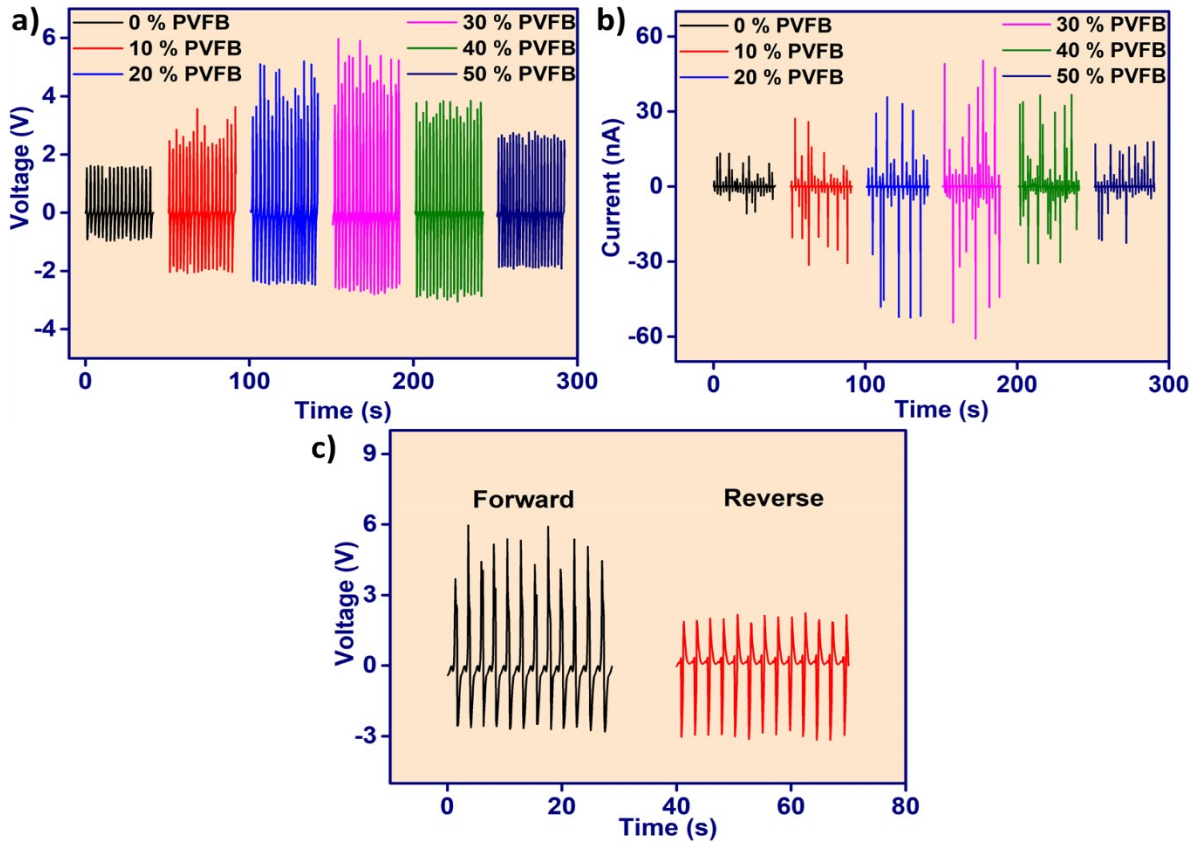

Figure S8 (a & b) The voltage and current response of unpoled PVFB PENGs under compressive force. **(c)** The switching polarity test of the 30 % PVFB PENG.

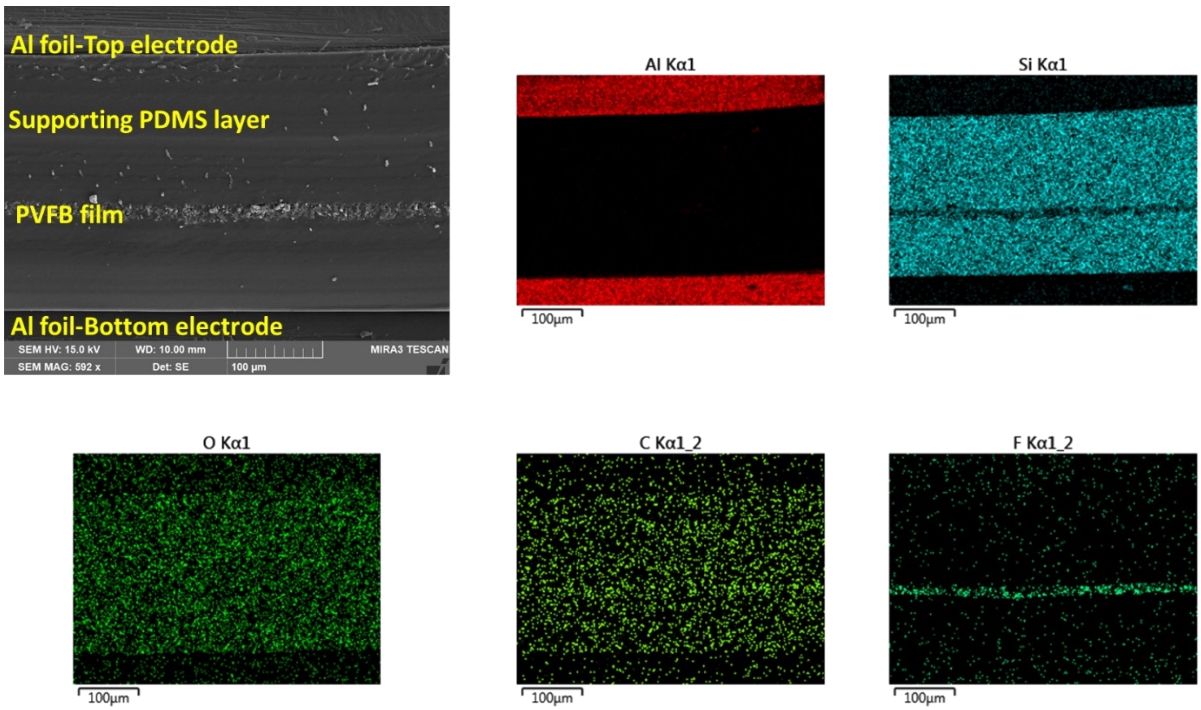

Figure S9 The cross-sectional SEM image of the 30 % PVFB film attached with the Al foil as electrodes with PDMS as supporting layer.

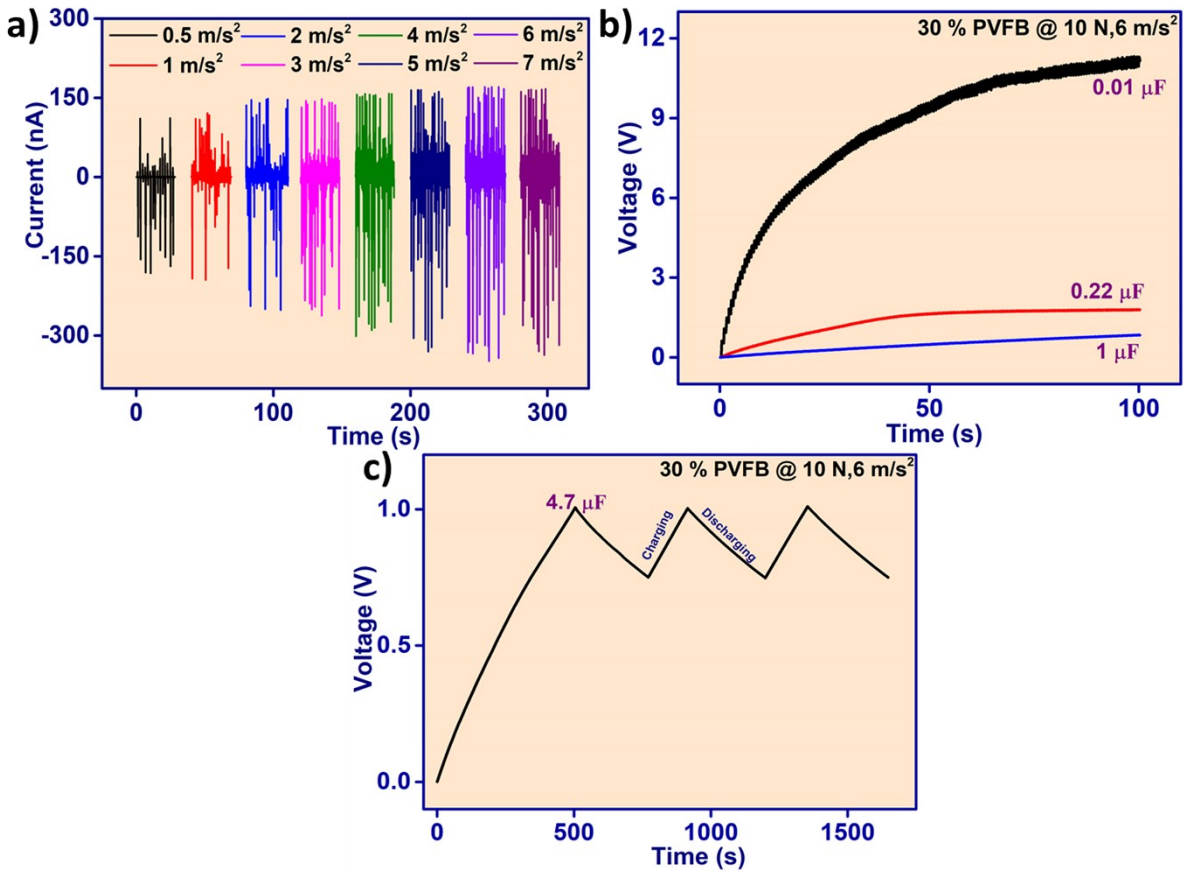

Figure S10 (a) The current response of 30 % poled PVFB PENG under various accelerations. (b The charging plot of 0.01, 0.22 and 1 µF capacitor using 30 % PVFB PENG up to 100 s. (c) The charging-discharging analysis of 4.7 µF using 30 % PVFB PENG.

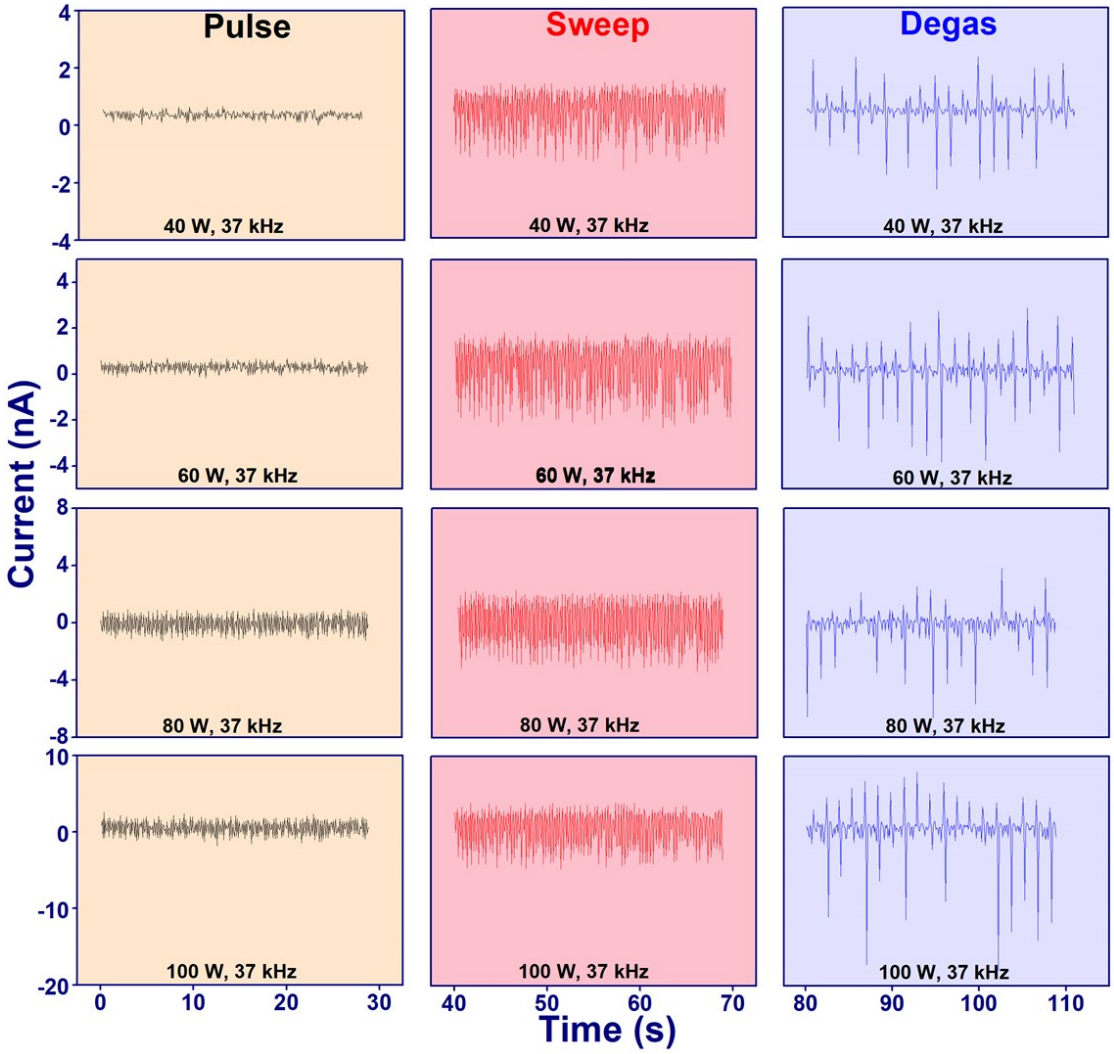

Figure S11 The current response of 30 % PVFB PENG under the varying power and sonicator operation modes.

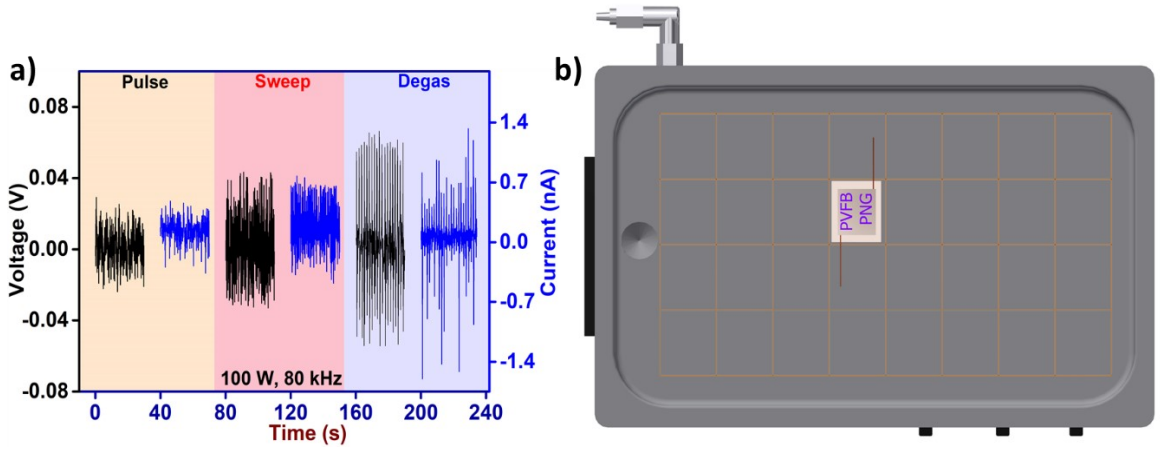

Figure S12 (a) The voltage and current response of 30 % PVFB PENG under 100 W power at 80 kHz with different sonicator operation modes. (b) The schematic diagram of 30 % PVFB PENG attachment on the surface of the bath sonicator as a sensing unit to identity the high active region.

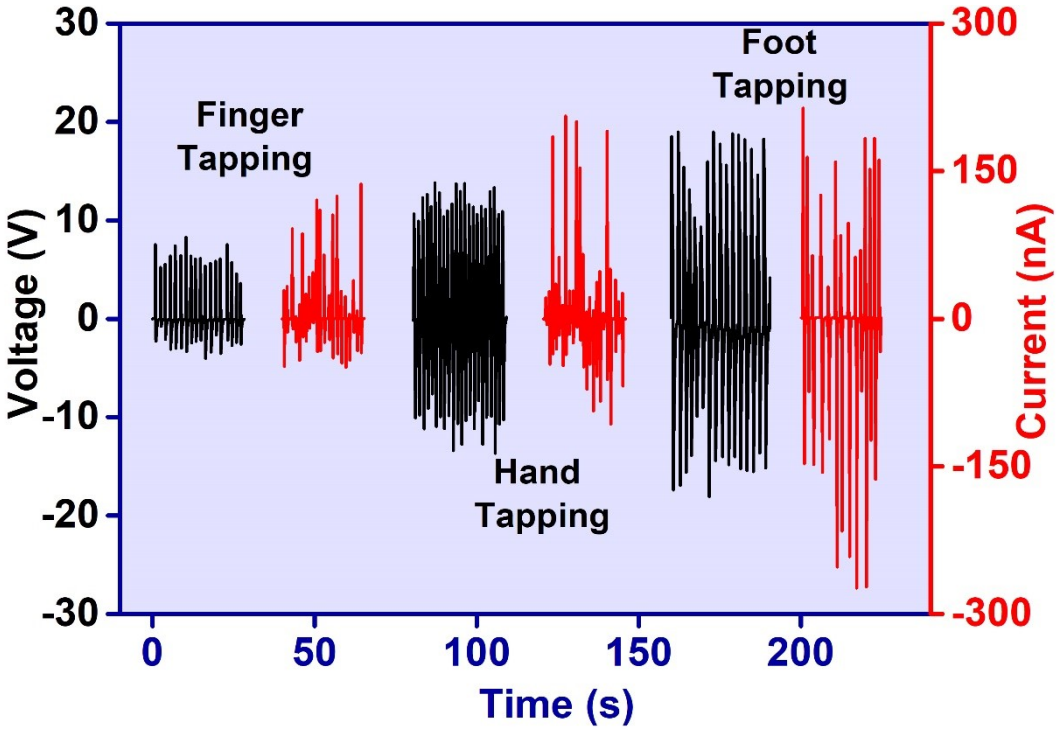

Figure S13 The electrical output of 30 % PVFB PENG under finger, hand and foot-tapping biomechanoid force conditions.

Polymer	Added Fillers	Preparation method	Solvent	Crystalline phase ~ (%)
PVDF-HFB [1]	-	Solution casting, Thermal induced phase separation (TIPS)	Dibutyl phthalate/ Dioctyl phthalate	27.70
PVDF-PEO [2]	-	Solution casting	DMF	43
PVDF [3]	$BaTiO_3$	Tape casting	DMF	49.8
PVDF [4]	ZnO	Tape casting	DMAc	37.26
PVDF [5]	-	Solution casting	DMAc	46
PVDF [6]	NiO	Solution casting	DMF	72
PVDF [7]	-	Thermal melting	-	39.18
PVDF [8]	$BaTiO_3$	Melt blending	-	52
PVDF [9]	A proportion of n-propanol, n-hexanol and glycerol mixture	Non-solvent induced phase separation (NIPS)	DMAc	60
		Melt spinning	-	48.7
		Solution casting	DMAc	70
PVDF [10]	Poly(ethyl methacrylate), PEMA	Melting blending	-	28
PVDF [11]	-	Melt compressed	-	39
		Solution casting	DMF	50
		Electrospun	DMF	47
PVDF [11]	1-allyl-3-methylimidazolium chloride	Melt compressed	-	44
		Solution casting	DMF	54

		Electrospun	DMF	52
PVDF [12]	-	Twin screw extruder @ 240°C	-	58
	Polyamide 6			32
PVDF [13]	-	Solution Casting -under magnetic field	DMF	49
PVDF [14]	-	Melt-Hot press	DMF	78
		Electrospinning	DMAc	56
PVDF-TrFE [15]	-	Solution casting	MEK	56
	$LiNbO_3$			67
PVDF [16]	-	Solution casting, TIPS	Methyl salicylate	47.7
PVDF-HFP Tri-layer [17]	Ni-ZnO	Solution casting	DMF/ Acetone	51.1
PVDF [18]	-	Solution casting, TIPS	DMC/ DMSO	15
	Protic ionic liquids			60
PVDF [19]		Solution casting	DMSO	50.9
PVDF [20]		Electrospinning	DMF/ Acetone	36.9
	Graphene			45.5
PVDF [21]	Poly(methyl methacrylate), PMMA	Spin coating	DMAc	45
PVDF [22]	-	Solution casting	DMAc	90
PVDF [23]	Polyethylene glycol in Ionic liquid	Solution casting	DMF	35
PVDF [24]	PMMA	Electrospinning	DMF/THF	50

PVDF [25]	Few layered graphene	Solution casting	DMF	53
	Graphene oxide			51
PVDF (Present work)	-	Tape casting, under 30 % RH	DMF	58.6
		Tape casting, under 60 % RH		75
	BNT			92

***DMAc: Dimethylacetamide, DMF: Dimethylformamide, THF: Tetrahydrofuran, MEK: Methyl Ethyl Ketone, DMC: Dimethyl carbonate, DMSO: Dimethyl sulfoxide.**

Table S1 The comparison table of the attained crystalline phase of PVFB with the recently reported articles on PVDF under various preparation techniques and added filler materials.

S.No	Material	~ d_{33}* (pm/V)	References
1	PVDF/BCZT	5	[26]
2	PVDF	49.6	[27]
3	PVDF	58	[28]
4	PVDF	30	[29]
5	PVDF	2	[30]
6	PVDF-TrFE	20	[31]
7	PVDF	43	[32]
8	PVDF	30	[33]
9	PVDF/CNT	35	
10	PVDF/Ag-CNTs	54	
11	PVDF	30	[34]
12	PVDF	20	[35]
13	PVDF/GO	110	
14	PVDF	28	[36]
15	PVDF	34	[37]
16	PVDF/$BaTiO_3$	48	[38]
17	PVDF	17.5	[39]
18	PVDF	49.6	[40]
19	PVDF-TrFE/GO	29.8	[41]
20	PVDF-TrFE	18	[42]
21	PVDF/Fluro doped Graphene	63	[43]
22	PVDF	64	[44]
23	PVDF/rGO	87	
24	PVDF	5	[45]
25	PVDF	144	[46]
26	PVDF	122	Present work
	PVDF/BNT	242	

***BCZT: $(BaCa)(ZrTi)O_3$, CNT: Carbon nanotubes, GO: Graphene oxide, BNT: $Na_{0.5}Bi_{0.5}TiO_3$.**

Table S2 The Comparison of piezoelectric coefficient values of as-prepared PVFB films with the recently reported PVDF and its copolymer coefficients.

Polymer	Added Fillers	Electrodes	Area (cm^2)	Applied force	Voltage ~ (V)	Current ~ (μA)
PVDF-TrFE [31]	-	Copper, Silver	-	-	9.5	-
PVDF [47]	rGO-Ag	Aluminum	13	BMF	18	1.05
PVDF [48]	-	-	5	-	10	-
	hBN				68	0.1
PVDF [49]	$BaTiO_3$	ITO	1	1000 N	150	1.5
PVDF-TrFE [50]	$BaTiO_3$	Aluminum	0.5	-	9	-
P(VDF-TrFE) [51]	BCZT	Gold		BMF	18	-
PVDF-TrFE [52]	-	Gold	-	-	2	0.9
	GO				4	1.8
PVDF [53]	BNNT	Silver, Gold	1	40 N	22	0.6
PVDF-TrFE [54]	KNN	ITO	-	-	0.8	0.08
PVDF [55]	$BaTiO_3$, Graphene	Aluminum	6.25	-	11	-
PVDF-TrFE [56]	$BaTiO_3$	Gold	-	-	13.2	0.3
PVDF-HFP [57]	ZnO	Aluminum	-	-	2.8	-
PVDF [58]		Aluminum	-	-	12	0.4
PVDF [59]	-	Aluminum	-	-	3.8	
	Graphene				7.9	
PVDF-HFP [60]	$BaTiO_3$, hBN	-	3.14	2.5 N	2.4	-
PVDF [61]	Graphene	-	12	BMF	11	0.006

PVDF [62]	ZnO, KNN	Aluminum	4	BMF	25	1.81
PVDF [63]	Platinum	Copper, Nickel	14	217 N	30	-
PVDF [64]	-	Aluminum	-	-	16	0.8
PVDF [65]	$BaTiO_3$	Aluminum	-	BMF	2	0.3
PVDF Present work	BNT	Aluminum	4	10 N	29.5	0.5

*** BMF: Biomechanical force, N: Newton, KNN: $K_{0.5}Na_{0.5}NbO_3$, hBN: hexagonal Boron nitride, BNNT: Boron nitride nanotubes.**

Table S3 The Energy harvesting performance comparison of PVFB PENGs with other recently reported PVDF and its copolymer-based piezoelectric nanogenerators.

References

[1] X. Wang, C. Xiao, H. Liu, Q. Huang, J. Hao, H. Fu, Poly (vinylidene fluoride-hexafluoropropylene) porous membrane with controllable structure and applications in efficient oil/water separation, Materials 11(3) (2018) 443.
[2] P. Dhatarwal, R. Sengwa, Tunable β-phase crystals, degree of crystallinity, and dielectric properties of three-phase PVDF/PEO/SiO2 hybrid polymer nanocomposites, Materials Research Bulletin 129 (2020) 110901.
[3] M. Sharma, J.K. Quamara, A. Gaur, Behaviour of multiphase PVDF in (1− x) PVDF/(x) BaTiO 3 nanocomposite films: structural, optical, dielectric and ferroelectric properties, Journal of Materials Science: Materials in Electronics 29(13) (2018) 10875-10884.
[4] E.R. Dyartanti, I.N. Widiasa, A. Purwanto, H. Susanto, Nanocomposite Polymer Electrolytes in PVDF/ZnO Membranes Modified with PVP for LiFePO_4 Batteries, Evergreen 5(2) (2018) 19-25.
[5] S. He, S. Zhai, C. Zhang, Y. Xue, W. Yang, J. Lin, Effect of Sulfonation Degree and PVDF Content on the Structure and Transport Properties of SPEEK/PVDF Blend Membranes, Polymers 11(4) (2019) 676.
[6] R.A. Amoresi, A.A. Felix, E.R. Botero, N.L. Domingues, E.A. Falcão, M.A. Zaghete, A.W. Rinaldi, Crystallinity, morphology and high dielectric permittivity of NiO nanosheets filling poly (vinylidene fluoride), Ceramics International 41(10) (2015) 14733-14739.
[7] G. He, T. Zhao, R. Sun, S. Yu, R. Du, Dielectric properties of Ni/poly (vinylidene fluoride) composites at high frequencies, 2010 11th International Conference on Electronic Packaging Technology & High Density Packaging, IEEE, 2010, pp. 452-455.
[8] N. Meng, R. Mao, W. Tu, K. Odolczyk, Q. Zhang, E. Bilotti, M.J. Reece, Crystallization kinetics and enhanced dielectric properties of free standing lead-free PVDF based composite films, Polymer 121 (2017) 88-96.
[9] J. Liu, X. Lu, C. Wu, Effect of preparation methods on crystallization behavior and tensile strength of poly (vinylidene fluoride) membranes, Membranes 3(4) (2013) 389-405.
[10] Z.-J. Huang, J. Jiang, G. Xue, D.-S. Zhou, β-Phase Crystallization of Poly (vinylidene fluoride) in Poly (vinylidene fluoride)/Poly (ethyl methacrylate) Blends, Chinese Journal of Polymer Science 37(1) (2019) 94-100.
[11] T. Pickford, X. Gu, E.L. Heeley, C. Wan, Effects of an ionic liquid and processing conditions on the β-polymorph crystal formation in poly (vinylidene fluoride), CrystEngComm 21(36) (2019) 5418-5428.
[12] N. Chen, X. Yao, C. Zheng, Y. Tang, M. Ren, Y. Ren, M. Guo, S. Zhang, L.-Z. Liu, Study on the miscibility, crystallization and crystalline morphology of polyamide-6/polyvinylidene fluoride blends, Polymer 124 (2017) 30-40.
[13] J. Wu, X. Sun, S. Zhu, J. Bai, X. Zhu, J. Dai, L. Yin, W. Song, Y. Sun, Magnetic field induced formation of ferroelectric β phase of poly (vinylidene fluoride), Applied Physics A 126(8) (2020) 1-6.
[14] J.Y. Lim, S. Kim, Y. Seo, Enhancement of β-phase in PVDF by electrospinning, AIP Conference Proceedings, AIP Publishing LLC, 2015, p. 070006.
[15] V. Strashilov, G. Alexieva, B. Vincent, V. Nguyen, D. Rouxel, Structural impact on piezoelectricity in PVDF and P (VDF-TrFE) thin films, Applied Physics A 118(4) (2015) 1469-1477.
[16] W. Ma, H. Yuan, X. Wang, The effect of chain structures on the crystallization behavior and membrane formation of poly (vinylidene fluoride) copolymers, Membranes 4(2) (2014) 243-256.

[17] H. Parangusan, D. Ponnamma, M.A.A. AlMaadeed, Flexible tri-layer piezoelectric nanogenerator based on PVDF-HFP/Ni-doped ZnO nanocomposites, RSC advances 7(79) (2017) 50156-50165.
[18] I. Vázquez-Fernández, A. Bouzina, M. Raghibi, L. Timperman, J. Bigarré, M. Anouti, Influence of hydrophilic/hydrophobic protic ionic liquids (PILs) on the poly (vinylidene fluoride)(PVDF-ionic liquid) membrane properties, Journal of Materials Science 55(35) (2020) 16697-16717.
[19] X. Li, Y. Wang, T. He, Q. Hu, Y. Yang, Preparation of PVDF flexible piezoelectric film with high β-phase content by matching solvent dipole moment and crystallization temperature, Journal of Materials Science: Materials in Electronics 30(22) (2019) 20174-20180.
[20] L. Jin, Y. Zheng, Z.-K. Liu, J.-S. Li, Y.-Y. Fan, L.-L. Xu, Y. Li, Enhancement of β-phase crystal content of poly (vinylidene fluoride) nanofiber web by graphene and electrospinning parameters, Chinese Journal of Polymer Science 38(11) (2020) 1239-1247.
[21] Y. Koseki, K. Aimi, S. Ando, Crystalline structure and molecular mobility of PVDF chains in PVDF/PMMA blend films analyzed by solid-state 19 F MAS NMR spectroscopy, Polymer journal 44(8) (2012) 757-763.
[22] R.E. Roy, S. Bhuvaneswari, K.P. Vijayalakshmi, R. Dimple, P.B. Soumyamol, R.S.N. Rajeev, Energy-induced polymorphic changes in poly (vinylidene fluoride): How ultrasonication results in polymer with predominantly γ phase, Journal of Polymer Science Part B: Polymer Physics 57(1) (2019) 40-50.
[23] P. Xu, W. Fu, Y. Hu, Y. Ding, Effect of annealing treatment on crystalline and dielectric properties of PVDF/PEG-containing ionic liquid composites, Composites Science and Technology 158 (2018) 1-8.
[24] Y.P. Mahant, S.B. Kondawar, D.V. Nandanwar, P. Koinkar, Poly (methyl methacrylate) reinforced poly (vinylidene fluoride) composites electrospun nanofibrous polymer electrolytes as potential separator for lithium ion batteries, Materials for Renewable and Sustainable Energy 7(2) (2018) 1-9.
[25] A. Islam, A.N. Khan, M.F. Shakir, K. Islam, Strengthening of β polymorph in PVDF/FLG and PVDF/GO nanocomposites, Materials Research Express 7(1) (2019) 015017.
[26] N. Enea, V. Ion, A. Moldovan, A. Bonciu, N.D. Scarisoreanu, Piezoelectric Hybrid Heterostructures PVDF/(Ba, Ca)(Zr, Ti) O3 Obtained by Laser Techniques, Coatings 10(12) (2020) 1155.
[27] G. Kalimuldina, N. Turdakyn, I. Abay, A. Medeubayev, A. Nurpeissova, D. Adair, Z. Bakenov, A Review of Piezoelectric PVDF Film by Electrospinning and Its Applications, Sensors 20(18) (2020) 5214.
[28] M. Kanik, O. Aktas, H.S. Sen, E. Durgun, M. Bayindir, Spontaneous high piezoelectricity in poly (vinylidene fluoride) nanoribbons produced by iterative thermal size reduction technique, ACS nano 8(9) (2014) 9311-9323.
[29] Y.-Y. Choi, P. Sharma, C. Phatak, D.J. Gosztola, Y. Liu, J. Lee, B. Lee, J. Li, A. Gruverman, S. Ducharme, Enhancement of local piezoresponse in polymer ferroelectrics via nanoscale control of microstructure, ACS nano 9(2) (2015) 1809-1819.
[30] M. Fortunato, H.C. Bidsorkhi, C.R. Chandraiahgari, G. De Bellis, F. Sarto, M.S. Sarto, PFM characterization of PVDF nanocomposite films with enhanced piezoelectric response, IEEE Transactions on Nanotechnology 17(5) (2018) 955-961.
[31] J.H. Kim, B. Kim, S.-W. Kim, H.W. Kang, M.-C. Park, D.H. Park, B.K. Ju, W.K. Choi, High-performance coaxial piezoelectric energy generator (C-PEG) yarn of Cu/PVDF-TrFE/PDMS/Nylon/Ag, Nanotechnology 32(14) (2021) 145401.
[32] P. Martins, C. Caparros, R. Gonçalves, P. Martins, M. Benelmekki, G. Botelho, S. Lanceros-Mendez, Role of nanoparticle surface charge on the nucleation of the electroactive

β-poly (vinylidene fluoride) nanocomposites for sensor and actuator applications, The Journal of Physical Chemistry C 116(29) (2012) 15790-15794.
[33] M. Sharma, V. Srinivas, G. Madras, S. Bose, Outstanding dielectric constant and piezoelectric coefficient in electrospun nanofiber mats of PVDF containing silver decorated multiwall carbon nanotubes: assessing through piezoresponse force microscopy, RSC advances 6(8) (2016) 6251-6258.
[34] Y. Huang, G. Rui, Q. Li, E. Allahyarov, R. Li, M. Fukuto, G.-J. Zhong, J.-Z. Xu, Z.-M. Li, P.L. Taylor, Enhanced piezoelectricity from highly polarizable oriented amorphous fractions in biaxially oriented poly (vinylidene fluoride) with pure β crystals, Nature communications 12(1) (2021) 1-8.
[35] A. Gebrekrstos, G. Madras, S. Bose, Journey of electroactive β-polymorph of poly (vinylidenefluoride) from crystal growth to design to applications, Crystal Growth & Design 19(9) (2019) 5441-5456.
[36] Y. Jiang, Y. Ye, J. Yu, Z. Wu, W. Li, J. Xu, G. Xie, Study of thermally poled and corona charged poly (vinylidene fluoride) films, Polymer Engineering & Science 47(9) (2007) 1344-1350.
[37] J. Gomes, J.S. Nunes, V. Sencadas, S. Lanceros-Méndez, Influence of the β-phase content and degree of crystallinity on the piezo-and ferroelectric properties of poly (vinylidene fluoride), Smart Materials and Structures 19(6) (2010) 065010.
[38] D.T. Le, S.J. Kwon, N.R. Yeom, Y.J. Lee, Y.H. Jeong, M.P. Chun, J.H. Nam, J.H. Paik, B.I. Kim, J.H. Cho, Effects of the Domain Size on Local d33 in Tetragonal (Na 0.53 K 0.45 Li 0.02)(Nb 0.8 Ta 0.2) O 3 Ceramics, Journal of the American Ceramic Society 96(1) (2013) 174-178.
[39] Y. Ting, H. Gunawan, A. Sugondo, C.-W. Chiu, A new approach of polyvinylidene fluoride (PVDF) poling method for higher electric response, Ferroelectrics 446(1) (2013) 28-38.
[40] N. Soin, D. Boyer, K. Prashanthi, S. Sharma, A.A. Narasimulu, J. Luo, T.H. Shah, E. Siores, T. Thundat, Exclusive self-aligned β-phase PVDF films with abnormal piezoelectric coefficient prepared via phase inversion, Chemical Communications 51(39) (2015) 8257-8260.
[41] M. Silibin, V. Bystrov, D. Karpinsky, N. Nasani, G. Goncalves, I. Gavrilin, A. Solnyshkin, P. Marques, B. Singh, I. Bdikin, Local mechanical and electromechanical properties of the P (VDF-TrFE)-graphene oxide thin films, Applied Surface Science 421 (2017) 42-51.
[42] G. Canavese, S. Stassi, V. Cauda, A. Verna, P. Motto, A. Chiodoni, S.L. Marasso, D. Demarchi, Different scale confinements of PVDF-TrFE as functional material of piezoelectric devices, IEEE Sensors Journal 13(6) (2013) 2237-2244.
[43] A. Gebrekrstos, G. Madras, S. Bose, Piezoelectric response in electrospun poly (vinylidene fluoride) fibers containing fluoro-doped graphene derivatives, ACS omega 3(5) (2018) 5317-5326.
[44] I.O. Pariy, A.A. Ivanova, V.V. Shvartsman, D.C. Lupascu, G.B. Sukhorukov, T. Ludwig, A. Bartasyte, S. Mathur, M.A. Surmeneva, R.A. Surmenev, Piezoelectric response in hybrid micropillar arrays of poly (vinylidene fluoride) and reduced graphene oxide, Polymers 11(6) (2019) 1065.
[45] M. Fortunato, C.R. Chandraiahgari, G. De Bellis, P. Ballirano, F. Sarto, A. Tamburrano, M.S. Sarto, Piezoelectric effect and electroactive phase nucleation in self-standing films of unpoled PVDF nanocomposite films, Nanomaterials 8(9) (2018) 743.
[46] N.R. Alluri, N.P. Maria Joseph Raj, G. Khandelwal, S.-J. Kim, High-Performance Multifaceted Piezoelectric Composite Nanogenerators for Weight-Monitoring Sensors, ACS Applied Electronic Materials 3(5) (2021) 2024-2034.

[47] M. Pusty, L. Sinha, P.M. Shirage, A flexible self-poled piezoelectric nanogenerator based on a rGO–Ag/PVDF nanocomposite, New Journal of Chemistry 43(1) (2019) 284-294.
[48] P. Yadav, T.D. Raju, S. Badhulika, Self-poled hBN-PVDF nanofiber mat-based low-cost, ultrahigh-performance piezoelectric nanogenerator for biomechanical energy harvesting, ACS Applied Electronic Materials 2(7) (2020) 1970-1980.
[49] Y. Zhao, Q. Liao, G. Zhang, Z. Zhang, Q. Liang, X. Liao, Y. Zhang, High output piezoelectric nanocomposite generators composed of oriented BaTiO3 NPs@ PVDF, Nano Energy 11 (2015) 719-727.
[50] S. Siddiqui, D.-I. Kim, M.T. Nguyen, S. Muhammad, W.-S. Yoon, N.-E. Lee, High-performance flexible lead-free nanocomposite piezoelectric nanogenerator for biomechanical energy harvesting and storage, Nano Energy 15 (2015) 177-185.
[51] J. Liu, B. Yang, L. Lu, X. Wang, X. Li, X. Chen, J. Liu, Flexible and lead-free piezoelectric nanogenerator as self-powered sensor based on electrospinning BZT-BCT/P (VDF-TrFE) nanofibers, Sensors and Actuators A: Physical (2020) 111796.
[52] V. Bhavanasi, V. Kumar, K. Parida, J. Wang, P.S. Lee, Enhanced piezoelectric energy harvesting performance of flexible PVDF-TrFE bilayer films with graphene oxide, ACS applied materials & interfaces 8(1) (2016) 521-529.
[53] S. Ye, C. Cheng, X. Chen, X. Chen, J. Shao, J. Zhang, H. Hu, H. Tian, X. Li, L. Ma, High-performance piezoelectric nanogenerator based on microstructured P (VDF-TrFE)/BNNTs composite for energy harvesting and radiation protection in space, Nano Energy 60 (2019) 701-714.
[54] H.B. Kang, C.S. Han, J.C. Pyun, W.H. Ryu, C.-Y. Kang, Y.S. Cho, (Na, K) NbO3 nanoparticle-embedded piezoelectric nanofiber composites for flexible nanogenerators, Composites Science and Technology 111 (2015) 1-8.
[55] K. Shi, B. Sun, X. Huang, P. Jiang, Synergistic effect of graphene nanosheet and BaTiO3 nanoparticles on performance enhancement of electrospun PVDF nanofiber mat for flexible piezoelectric nanogenerators, Nano Energy 52 (2018) 153-162.
[56] X. Chen, X. Li, J. Shao, N. An, H. Tian, C. Wang, T. Han, L. Wang, B. Lu, High-performance piezoelectric nanogenerators with imprinted P (VDF-TrFE)/BaTiO3 nanocomposite micropillars for self-powered flexible sensors, Small 13(23) (2017) 1604245.
[57] H. Parangusan, D. Ponnamma, M.A.A. Al-Maadeed, Stretchable electrospun PVDF-HFP/Co-ZnO nanofibers as piezoelectric nanogenerators, Scientific reports 8(1) (2018) 1-11.
[58] S. Bhattacharjee, S. Mondal, A. Banerjee, K.K. Chattopadhyay, Dielectric and piezoelectric augmentation in self-poled magnetic Fe3O4/poly (vinylidene fluoride) composite nanogenerators, Materials Research Express 7(4) (2020) 044001.
[59] M.M. Abolhasani, K. Shirvanimoghaddam, M. Naebe, PVDF/graphene composite nanofibers with enhanced piezoelectric performance for development of robust nanogenerators, Composites Science and Technology 138 (2017) 49-56.
[60] D. Ponnamma, M.A.A. Al-Maadeed, Influence of BaTiO 3/white graphene filler synergy on the energy harvesting performance of a piezoelectric polymer nanocomposite, Sustainable energy & fuels 3(3) (2019) 774-785.
[61] S. Garain, S. Jana, T.K. Sinha, D. Mandal, Design of in situ poled Ce3+-doped electrospun PVDF/graphene composite nanofibers for fabrication of nanopressure sensor and ultrasensitive acoustic nanogenerator, ACS applied materials & interfaces 8(7) (2016) 4532-4540.
[62] S. Bairagi, S.W. Ali, A hybrid piezoelectric nanogenerator comprising of KNN/ZnO nanorods incorporated PVDF electrospun nanocomposite webs, International Journal of Energy Research 44(7) (2020) 5545-5563.

[63] S.K. Ghosh, D. Mandal, Synergistically enhanced piezoelectric output in highly aligned 1D polymer nanofibers integrated all-fiber nanogenerator for wearable nano-tactile sensor, Nano Energy 53 (2018) 245-257.
[64] D.W. Lee, D.G. Jeong, J.H. Kim, H.S. Kim, G. Murillo, G.-H. Lee, H.-C. Song, J.H. Jung, Polarization-controlled PVDF-based hybrid nanogenerator for an effective vibrational energy harvesting from human foot, Nano Energy 76 (2020) 105066.
[65] H.H. Singh, M. Singh, K. Gangwal, M. Faraz, N. Khare, BaTiO3-PVDF composite film for piezoelectric nanogenerator, AIP Conference Proceedings, AIP Publishing LLC, 2020, p. 030642.